Composites Communications 46 (2024) 101804

Contents lists available at ScienceDirect

Composites Communications

journal homepage: www.elsevier.com/locate/coco

Short Communication

Micro-crosslinked polyimide nanocomposites with low dielectric constant and low dielectric loss for microwave antenna with molecular dynamics

Zhiyuan Peng [a], An Ye [b], Ling Zhang [a,*], Xiaolin Li [b], Cheng Lian [c], Chunzhong Li [a,**]

[a] Key Laboratory for Ultrafine Materials of Ministry of Education, Shanghai Engineering Research Center of Hierarchical Nanomaterials, Frontiers Science Center for Materiobiology and Dynamic Chemistry, School of Materials Science and Engineering, East China University of Science and Technology, Shanghai, 200237, PR China
[b] School of Physics, East China University of Science and Technology, Shanghai, 200237, PR China
[c] State Key Laboratory of Chemical Engineering, School of Chemical Engineering, East China University of Science and Technology, Shanghai, 200237, PR China

ARTICLE INFO

Keywords:
Polyimide
Polyhedral oligomeric silsesquioxane
Low dielectric
Molecular dynamics

ABSTRACT

Low dielectric polyimide (PI) is a crucial component of interlayer dielectric materials in modern electronic devices, which effectively mitigates signal delay and power loss issues arising from the high integration. Herein, low dielectric nanocomposite with micro-crosslinked structure is prepared through in-situ polymerization of fluorinated PI (f-PI) and polyhedral oligomeric silsesquioxane (POSS). Four f-PIs with different positions of trifluoromethyl and structure of backbone, and three functionalized POSS are studied by density functional theory (DFT) and classical molecular dynamics (MD) simulations to reveal the effects of the PI structure and the interfacial interaction of POSS with PI on dielelectric constant. Specifically, the dielectric constant and dielectric loss of 3 wt% 8NH_2-POSS/PI1 at 1 kHz are reduced to 2.40 and 0.0017, respectively. The micro-crosslinked structure provides better thermal stability (513.3 °C), coefficient of thermal expansion (42.14 ppm $°C^{-1}$), and acid resistance, meeting the requirements of integrated circuits (ICs) processing. In comparison to commercial epoxy boards (FR4), the 3 wt% 8NH_2-POSS/PI exhibits lower S_{11} signal loss (−10.874 dB) and provides greater magnetic fields (2.00 G) near 3.0 GHz as the substrate of Nitrogen-Vacancy (NV) centers sensor. This well-performing low dielectric nanocomposite offers a promising medium for ICs.

1. Introduction

Polyimide (PI) is a kind of special engineering plastic known for its excellent electrical insulation, thermal stability, mechanical strength and chemical inertness [1]. Nowadays, PI has become the primary interlayer insulating material, finding extensive applications in communication information [2], integrated circuits [3], microelectromechanical systems [4], liquid crystal displays [5], lithography [6] and aerospace [7]. However, the integration of microelectronic devices entails parasitic capacitance, urgently requiring novel PI with low dielectric constant ($\varepsilon < 2.5$) and ultra-low dielectric loss ($\tan\delta < 0.005$) to alleviate the problem of power consumption and signal crosstalk [8–10].

According to the Clausius-Mossotti formula $\frac{\varepsilon-1}{\varepsilon+1} = \frac{N\alpha}{3\varepsilon_0}$, where α, N and ε_0 represent the molecular polarizability, the number of polarized molecules per unit volume and ε of vacuum, respectively [11], decreasing polarizability and increasing free volume are effective approaches to reduce ε of polymers [12,13]. The introduction of fluorine-containing groups, particularly trifluoromethyl with low polarization rate and large bulk effect, proves to reduce the intrinsic ε significantly [14–16]. Yang et al. separately synthesized trifluoromethyl-containing 6FDAM, 12FDA and 15FDA diamine, and demonstrated a linear decrease in the corresponding ε of these PIs as the mass fraction of fluorine atoms in repeating unit (F%) increased [17]. Yi Zhang et al. utilizing an artificial neural network, identified that the optimal F% fell within the range from 25 % to 37 % [18]. However, only using F% to access ε is an incomplete approach [19,20], because the position of substitutions and structure of backbone also have great effects on ε. Until now, there has been a lack of systematic conclusions on the factors influencing ε of polymers, especially at the atomic level. Moreover, doping POSS increases free volume without encountering water absorption or surface roughness [21–24], commonly used to reduce ε. The customizable functional groups in POSS necessitate comprehensive investigation due to their direct impact on the dispersion

* Corresponding author.
** Corresponding author.
E-mail addresses: zlingzi@ecust.edu.cn (L. Zhang), czli@ecust.edu.cn (C. Li).

https://doi.org/10.1016/j.coco.2023.101804
Received 16 September 2023; Received in revised form 25 December 2023; Accepted 28 December 2023
Available online 6 January 2024

Composites Communications 46 (2024) 101804

Contents lists available at ScienceDirect

Composites Communications

journal homepage: www.elsevier.com/locate/coco

Short Communication

Micro-crosslinked polyimide nanocomposites with low dielectric constant and low dielectric loss for microwave antenna with molecular dynamics

Zhiyuan Peng [a], An Ye [b], Ling Zhang [a,*], Xiaolin Li [b], Cheng Lian [c], Chunzhong Li [a,**]

[a] Key Laboratory for Ultrafine Materials of Ministry of Education, Shanghai Engineering Research Center of Hierarchical Nanomaterials, Frontiers Science Center for Materiobiology and Dynamic Chemistry, School of Materials Science and Engineering, East China University of Science and Technology, Shanghai, 200237, PR China
[b] School of Physics, East China University of Science and Technology, Shanghai, 200237, PR China
[c] State Key Laboratory of Chemical Engineering, School of Chemical Engineering, East China University of Science and Technology, Shanghai, 200237, PR China

ARTICLE INFO

Keywords:
Polyimide
Polyhedral oligomeric silsesquioxane
Low dielectric
Molecular dynamics

ABSTRACT

Low dielectric polyimide (PI) is a crucial component of interlayer dielectric materials in modern electronic devices, which effectively mitigates signal delay and power loss issues arising from the high integration. Herein, low dielectric nanocomposite with micro-crosslinked structure is prepared through in-situ polymerization of fluorinated PI (f-PI) and polyhedral oligomeric silsesquioxane (POSS). Four f-PIs with different positions of trifluoromethyl and structure of backbone, and three functionalized POSS are studied by density functional theory (DFT) and classical molecular dynamics (MD) simulations to reveal the effects of the PI structure and the interfacial interaction of POSS with PI on dielelectric constant. Specifically, the dielectric constant and dielectric loss of 3 wt% $8NH_2$-POSS/PI1 at 1 kHz are reduced to 2.40 and 0.0017, respectively. The micro-crosslinked structure provides better thermal stability (513.3 °C), coefficient of thermal expansion (42.14 ppm $°C^{-1}$), and acid resistance, meeting the requirements of integrated circuits (ICs) processing. In comparison to commercial epoxy boards (FR4), the 3 wt% $8NH_2$-POSS/PI exhibits lower S_{11} signal loss (−10.874 dB) and provides greater magnetic fields (2.00 G) near 3.0 GHz as the substrate of Nitrogen-Vacancy (NV) centers sensor. This well-performing low dielectric nanocomposite offers a promising medium for ICs.

1. Introduction

Polyimide (PI) is a kind of special engineering plastic known for its excellent electrical insulation, thermal stability, mechanical strength and chemical inertness [1]. Nowadays, PI has become the primary interlayer insulating material, finding extensive applications in communication information [2], integrated circuits [3], micro-electromechanical systems [4], liquid crystal displays [5], lithography [6] and aerospace [7]. However, the integration of microelectronic devices entails parasitic capacitance, urgently requiring novel PI with low dielectric constant ($\varepsilon < 2.5$) and ultra-low dielectric loss ($\tan\delta < 0.005$) to alleviate the problem of power consumption and signal crosstalk [8–10].

According to the Clausius-Mossotti formula $\frac{\varepsilon-1}{\varepsilon+1} = \frac{N\alpha}{3\varepsilon_0}$, where α, N and ε_0 represent the molecular polarizability, the number of polarized molecules per unit volume and ε of vacuum, respectively [11], decreasing polarizability and increasing free volume are effective approaches to reduce ε of polymers [12,13]. The introduction of fluorine-containing groups, particularly trifluoromethyl with low polarization rate and large bulk effect, proves to reduce the intrinsic ε significantly [14–16]. Yang et al. separately synthesized trifluoromethyl-containing 6FDAM, 12FDA and 15FDA diamine, and demonstrated a linear decrease in the corresponding ε of these PIs as the mass fraction of fluorine atoms in repeating unit (F%) increased [17]. Yi Zhang et al. utilizing an artificial neural network, identified that the optimal F% fell within the range from 25 % to 37 % [18]. However, only using F% to access ε is an incomplete approach [19,20], because the position of substitutions and structure of backbone also have great effects on ε. Until now, there has been a lack of systematic conclusions on the factors influencing ε of polymers, especially at the atomic level. Moreover, doping POSS increases free volume without encountering water absorption or surface roughness [21–24], commonly used to reduce ε. The customizable functional groups in POSS necessitate comprehensive investigation due to their direct impact on the dispersion

* Corresponding author.
** Corresponding author.
E-mail addresses: zlingzi@ecust.edu.cn (L. Zhang), czli@ecust.edu.cn (C. Li).

https://doi.org/10.1016/j.coco.2023.101804
Received 16 September 2023; Received in revised form 25 December 2023; Accepted 28 December 2023
Available online 6 January 2024

of fillers and dielectric properties of nanocomposites [25,26].

In this work, low ε nanocomposites based on f-PI and functionalized POSS with excellent overall performance are prepared as advanced microwave antenna substrates. Four f-PI repeating units with four trifluoromethyl yet different structure are synthesized, and the F% range from 24.62 % to 31.32 %, within the suitable F% range for low ε PI [18]. The relationship between PI structure and ε is deeply studied through analyzing the four factors (polarization rate, dipole moment, fractional free volume (FFV) and interaction with water) by DFT and MD simulations. Suitable functionalized POSS is screened by compatibility and interfacial trapping effect with PI matrix, followed by in-situ polymerization to form micro-crosslinked structure. The resultant nanocomposite (3 wt% 8NH_2-POSS/PI1) exhibits low ε, ultra-low dielectric loss, and satisfies all conditions for high-temperature IC processing. As the

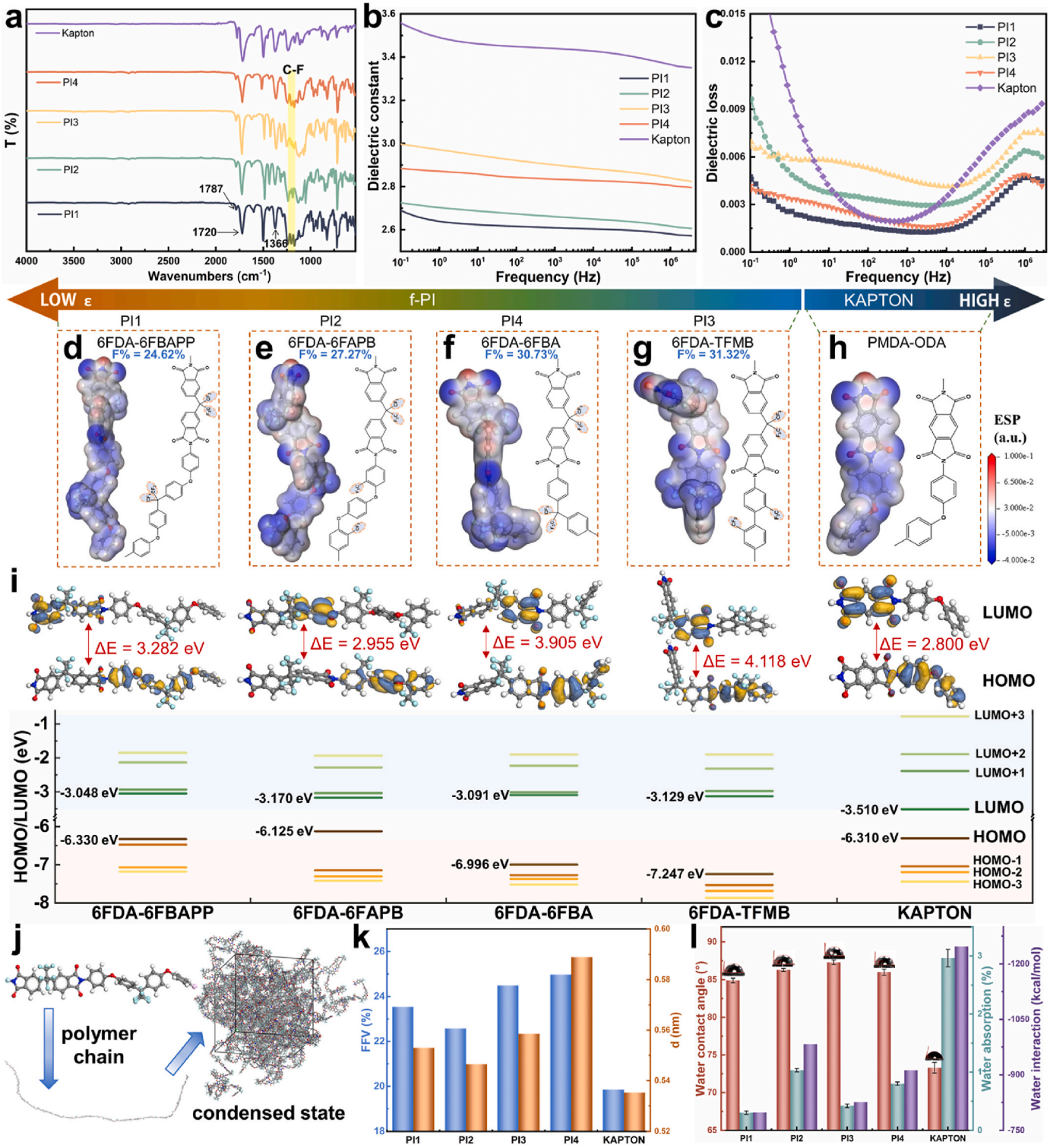

Fig. 1. a) FTIR, b) dielectric constant and c) dielectric loss of PIs. Electrostatic potential maps of d) 6FDA-6FBAPP, e) 6FDA-6FAPB, f) 6FDA-6FBA, g) 6FDA-TFMB, h) PMDA-ODA. i) LUMO, HOMO distribution and energy diagram of PIs. j) Process of polymer system construction. k) FFV, average intermolecular chain spacing, l) water contact angle, moisture rate and interaction with water of PI systems.

microwave antenna for Nitrogen-Vacancy centers sensor, 3 wt% $8NH_2$-POSS/PI1 exhibits lower signal loss and higher magnetic field than commercial printed circuit boards.

2. Results and discussion

2.1. Preparation and analysis of PIs with low dielectric constant

f-PIs are synthesized via four diamine monomers: 6FBAPP, 6FAPB, TFMB and 6FBA with the same dianhydride monomer 6FDA as described in Scheme S1. In Fig. 1a, peaks at 1787 and 1720 cm^{-1} correspond to the asymmetric and symmetric vibration of C═O in imide rings, respectively, while peak at 1366 cm^{-1} corresponds to the C–N stretching [27]. Meanwhile, the characteristic peaks for N–H of PAA at around 1550 and 3000 cm^{-1} are not observed, indicating the complete imidization of f-PIs [28]. The ^1H NMR of PI1 in Fig. S1a also demonstrates its successful synthesis.

The ε of all f-PIs in Fig. 1b are less than 3.0 over the measurement range, and significantly lower than ε of Kapton (3.4). PI1 exhibits the lowest ε (2.61 at 1 kHz) and low dielectric loss (Fig. 1c) with relatively low F% (24.62 %) among f-PIs, which is not consistent with traditional perception [17]. Therefore, factors influencing ε of polymers need to be evaluated more essentially and comprehensively.

The ε expresses the ability of materials to polarize in response to an applied field, where the structure with low polarization rate and dipole moment can reduce intrinsic ε [29]. The electrostatic potential maps of these PIs with different repeating units are depicted in Fig. 1d–h, where blue regions correspond to negative potential regions. The blue regions surrounding trifluoromethyl reduce the density of the electron cloud on the adjacent benzene ring and impede the free delocalization of the π electron, thereby weakening the polarization rate of benzene ring generated in the electric field [30]. Due to stronger electrophilicity and colossal steric hindrance of trifluoromethyl, f-PIs present a much larger LUMO-HOMO gap and denser molecular orbital distribution than Kapton (Fig. 1i), which mitigates intermolecular charge transfer complex (CTC) effects [31,32], thereby reducing the dipole moment. The values of polarizability and dipole moment per unit volume for these PIs are listed in Table S1, where PI1 exhibits both the minimum values, attributed to more electronegative groups (-O-, $–CF_3$) and more symmetrical backbone in structure.

Ambient air and water also have effects on ε of polymers, where increasing air ($\varepsilon = 1$) and decreasing water ($\varepsilon = 81$) of polymer condensed states help to reduce ε. The bulk-effect trifluoromethyl groups increase the average spacing of molecular chains and torsion angle of the bond between adjacent benzene rings in f-PI, leading to larger FFV to accommodate sub-nanometer air (Fig. 1k–S2 and S3). The larger FFV of f-PIs does not cause excessive diffusion of water because of the hydrophobicity of trifluoromethyl. Fig. 1l illustrates that the water contact angle, representing the initial hydrophobicity, increases with higher F%. However, in long-term tests, PI1 with more water-repellent beneze rings exhibits the lowest water absorption rate (0.30 %), which is also demonstrated by MD interaction energy (Fig. S4). In summary, PI1 exhibits the lowest ε among these PIs with ultra-low conductivity and good transmission (Fig. S1), suitable as low ε matrix and expanding its applications in optoelectronics.

2.2. Screening and synthesis of POSS nanoparticles

Hollow-cage POSS nanoparticles with appropriate functional groups can further reduce the ε of PI1 and improve overall performance [33,34]. Three distinct functionalized POSS with PI1 are constructed to simulate multiphase structure, which are TrisilanolPhenyl-POSS (Phenyl-POSS), TrisilanolIsobutyl-POSS (Isobutyl-POSS) and OctaAminopropyl-POSS ($8NH_2$-POSS). The calculated interaction energy by DFT between these POSS and PI1 monomer is illustrated in Fig. S5a, wherein higher interaction energy of $8NH_2$-POSS/PI1 leads to better compatibility [35]. Compared to phenyl and isobutyl, the aminopropyl group is more polar and produces stronger interaction with polar PI1 [36]. The electrostatic potentials (ESP) of POSS/PI1 are depicted in Fig. 2a–c, where ESP around aminopropylheptyl in $8NH_2$-POSS shows negative potential, indicating the deepest trapping effect in the interface sites with the same negatively charged PI1. Consequently, $8NH_2$-POSS/PI1 restrains the charge carriers injection and migration [37,38], thereby lowing ε of nanocomposites. Furthermore, incorporating $8NH_2$-POSS enhances the FFV of nanocomposites and reduces water interaction (Figs. S5b and S5c), resulting in a positive effect on ε reduction.

$8NH_2$-POSS is prepared by hydrolytic polycondensation of silane using γ-aminopropyltriethoxysilane as the precursor and purified through solvent crystallization. Fig. 2d–f demonstrate that the peaks are attributed to the carbon and hydrogen signal of organic functional groups at polyhedral vertices, with only one type of silicon atom in the structural conformation. In addition, −67 ppm of chemical shifts are close to those of silicon atoms in the cage structure of $(RSiO_{1.5})_8$ [39]. Fewer spurious peaks also prove that the product is a uniform structure with high purity. The structure of $8NH_2$-POSS is further supported by FTIR spectrum and elemental mapping images in Fig. S6. The broad peak at 3360 cm^{-1} is the result of the characteristic absorption of $–NH_2$ groups and bonding water [40]. The weight loss before 150 °C in Fig. S6b is caused by the condensation of crystalline water and silicone hydroxyl groups. Double bands at 2932 and 2876 cm^{-1} correspond to the C–H stretching [41]. The peaks at 1125, 1030 and 860 cm^{-1} are attributed to the vibration of the *Si*–O–Si framework [42].

2.3. Characterization and performance of nanocomposites

$8NH_2$-POSS nanoparticles are introduced into the PI1 matrix by in-situ polymerization forming micro-crosslinked structure. In contrast, commercial aminopropyllsobutyl POSS (NH_2-POSS) is compounded with PI1 as a comparison sample with non-crosslinked structure (Fig. S7). Two nanocomposites are individually immersed in concentrated sulfuric acid at 50 °C, and 3 wt% NH_2-POSS/PI1 shows apparent dissolution within 8 h, while 3 wt% $8NH_2$-POSS/PI1 is completely free of dissolution and crumple during one month in Fig. S8. The crosslinking density of 3 wt% $8NH_2$-POSS/PI1 increases to 0.745×10^3 mol m^{-3}, which is about 3 times higher than that of 3 wt% NH_2-POSS/PI1, leading to the higher glass transition temperature (Tg) of 269.0 °C and smaller mean squared displacement of 3 wt% $8NH_2$-POSS/PI1, demonstrating stronger interaction in $8NH_2$-POSS/PI1 system (Fig. S9).

The ε of the PI nanocomposites gradually decreases with increasing $8NH_2$-POSS content and 3 wt% $8NH_2$-POSS/PI1 reaches low ε value of 2.40 at 1 kHz and 2.24 at 3 GHz in Fig. 3a and S10. The symmetrical structure of $8NH_2$-POSS with hollow cage structure has an extremely low intrinsic polarity. Moreover, as the degree of crosslinking increases, stronger interactions weaken the motion of the polar orientation and relaxation [43]. Compared with 3 wt% NH_2-POSS/PI1, 3 wt% $8NH_2$-POSS/PI1 has a higher ε in low-frequency region, because of the closer chain segment spacing of 3 wt% $8NH_2$-POSS/PI1 and smaller FFV (Fig. S11) leading to a decreased amount of sub-nanometer air within the composites. But the gap between the two curves becomes progressively smaller in high-frequency regions and exhibits lower ε above 1 MHz, where a greater degree of chain entanglements in micro-crosslinked structure hinders the orientation of dipoles in high-frequency electric fields [44]. The addition of $8NH_2$-POSS reduces the dielectric loss of nanocomposite in high-frequency region (Fig. 3b) for good compatibility between $8NH_2$-POSS and PI1 resulting in few interfacial loss between them [45]. The dielectric strength of PI1 and hybrids are analyzed by Weibull distribution. The characteristic breakdown strengths (E_0) and shape distribution parameter (β) are calculated by Weibull distribution in Fig. 3c, where E_0 of 3 wt% $8NH_2$-POSS/PI1 (249.5 kV mm^{-1}) is approximately 30 % higher than that of PI1 with best stability, which indicates superior dielectric strength and insulation

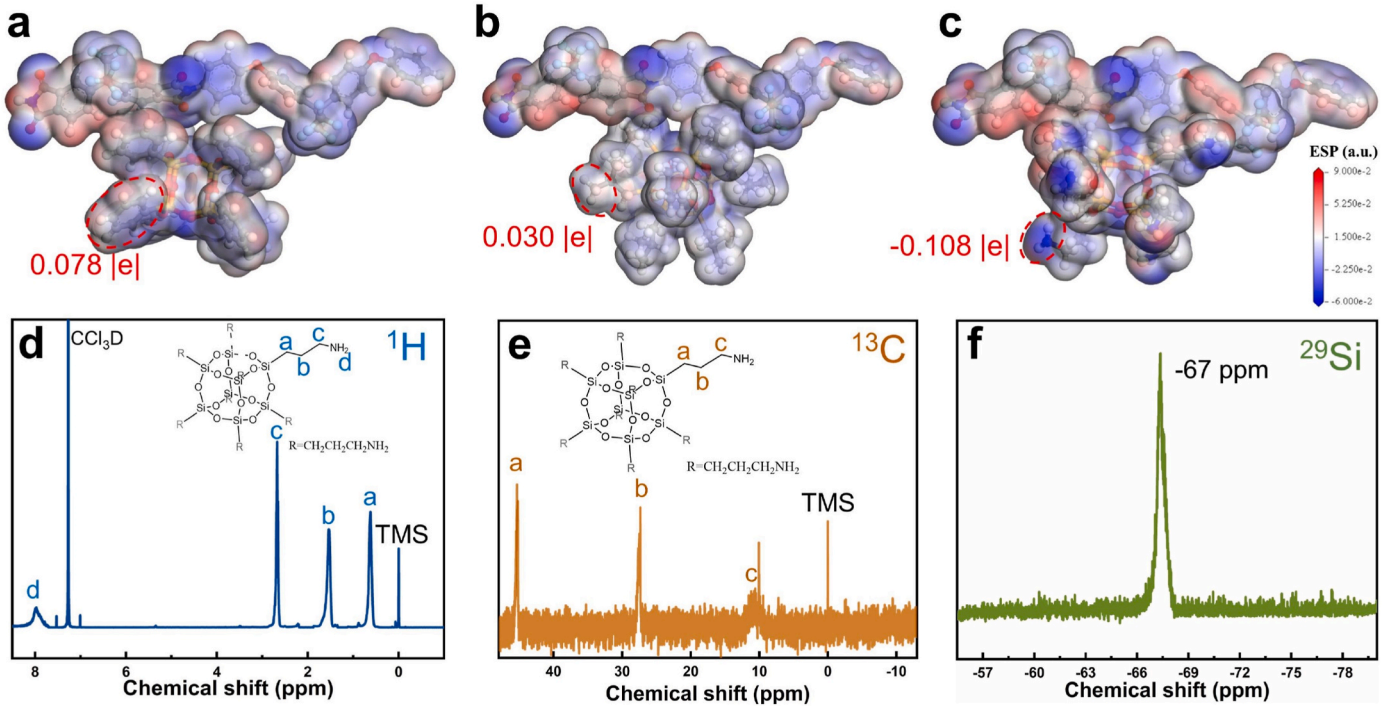

Fig. 2. Electrostatic potential diagram of a) Phenyl-POSS/PI1, b) Isobutyl-POSS/PI1 and c) 8NH_2-POSS/PI1. d) ^{1}H NMR, e) ^{13}C NMR, f) ^{29}*Si*-NMR and of 8NH_2-POSS.

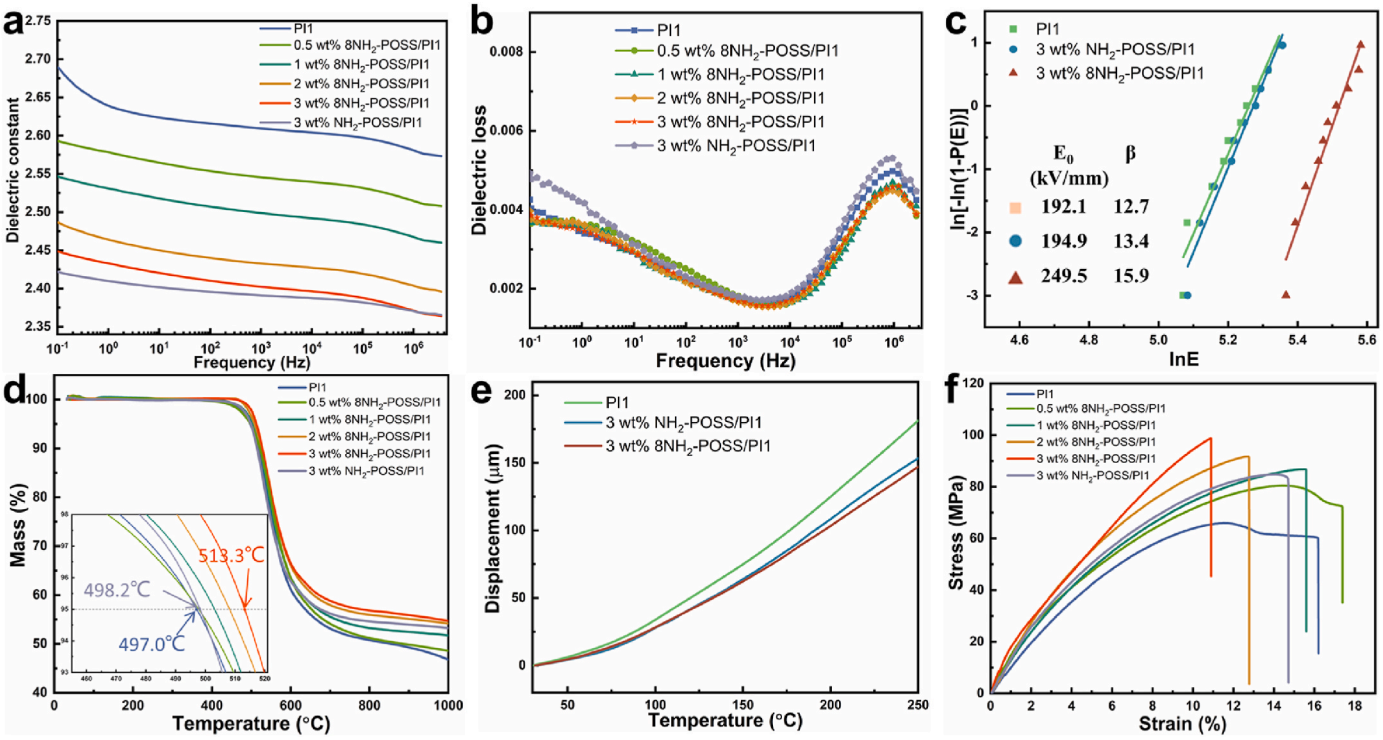

Fig. 3. a) Dielectric constant, b) dielectric loss, d) TGA of PI1 and f) tensile stress-strain curves of PI1 matrix and nanocomposite. c) Weibull distribution and e) DMA curves of PI1, 3 wt% NH_2-POSS/PI1 and 3 wt% 8NH_2-POSS/PI1.

capacity. The crosslinked structure mitigates damage caused by thermal and partial discharge breakdown [46]. The 5 wt% weight loss temperature ($T_{5\%}$) of 3 wt% 8NH_2-POSS/PI1 is about 513.3 °C, 16.3 °C higher than $T_{5\%}$ of pure PI1 (Fig. 3d), while 3 wt% 8NH_2-POSS/PI1 exhibits the lowest coefficient of thermal expansion (CTE = 42.14 ppm °C^{-1}) caluclated by DMA curves in Fig. 3e and Table S2, achieving the performance as wafer-level packaging [15]. As the 8NH_2-POSS content increases, mechanical strength and modulus gradually improve due to the greater degree of crosslinking as presented in Fig. 3f. 3 wt% 8NH_2-POSS/PI1 reaches 98.81 MPa, 59.37 % and 16.66 % higher than that of PI1 and 3 wt% NH_2-POSS/PI1, respectively. The rougher fracture cross-section of 3 wt% 8NH_2-POSS/PI1 in Fig. S12 also demonstrates

stronger interactions and greater stress transfer capability of 3 wt% $8NH_2$-POSS/PI1. Besides, the introduction of POSS further improves the optical transmittance of films (Fig. S13).

2.4. Microwave antenna application

Durable substrates for flexible devices need to withstand repeated folding and have good adhesion to conductors [47,48]. In Fig. 4a, the resistance of the circuit remains almost constant after 3000 folding cycles over 150°. After 20,000 folding cycles, there is only a 6.2 % variation in resistance, demonstrating good reliability of 3 wt% $8NH_2$-POSS/PI1. The scattering parameters, such as transmission coefficient (S_{11}) and reflection coefficient (S_{21}), represent the signal-transmitting efficiency of the circuit (Fig. S14). In circuit 1, S_{21} of $8NH_2$-POSS/PI1 is higher and smoother than the S_{21} of the FR4 substrate at frequencies above 0.3 GHz, and the first peak of POSS/PI1 is −26.61 dB, showing an improvement of ~5 dB (Fig. 4b). Circuit 2 is a microwave antenna that can be applied to Nitrogen-Vacancy (NV) centers, which are typical luminous point defects in diamond with the characterization of excellent spin properties [49]. NV centers serve as promising quantum sensors for temperature [50], electric field [51], magnetic field [52] and pressure [53] with high spatial resolution and high sensitivity. Given the diamond NV centers have a zero-field splitting at 2.87 GHz, performance differences around 3.0 GHz are especially emphasized. The peak S_{11} of $8NH_2$-POSS/PI1 in Fig. 4c is −10.874 dB, while that of FR4 is −7.786 dB. Simultaneously, as verified by the finite element method in Fig. 4d, $8NH_2$-POSS/PI1 substrate results in an S_{11} performance improvement of ~29 % to FR4 substrate near 3.0 GHz. The lower S_{11} of $8NH_2$-POSS/PI1 in high frequency denotes strong radiation and easy integration, which can generate stronger magnetic fields, enhancing the signal strength to efficiently modulate the NV centers. The simulated average magnetic field amplitude along the central x-axis and y-axis excited by POSS/PI1 in the xy-plane at the bottom of the 4 × 4 × 4 mm square (Fig. 4e) reaches 2006.90 mG, which is much stronger than the amplitude on the FR4 substrate (105.62 mG) at 3.0 GHz (Fig. 4f and S15), contributing to the development of compact and powerful NV centers-based magnetic measurement devices.

3. Conclusion

In summary, 6FDA-6FBAPP (PI1) exhibits the lowest polarization rate, dipole moment, water absorption, and higher FFV accommodating air, making it suitable for the matrix as low ε PI composites. Next, $8NH_2$-POSS is screened for better compatibility and interfacial trapping effect with PI1. Following in-situ polymerization, 3 wt% $8NH_2$-POSS/PI1 demonstrates excellent dielectric properties and meets the necessary conditions required for IC processing due to its micro-crosslinked structure. The ε and dielectric loss of 3 wt% $8NH_2$-POSS/PI1 reach 2.40 and 0.00170 at 1 kHz, leading to the lower signal loss (S_{11} = −10.874 dB) and stronger magnetic field (2.00 G) at operating frequency compared to commercial FR4 substrates as NV centers sensor. Compared to non-crosslinked 3 wt% NH_2-POSS/PI1, micro-crosslinked structure provides better acid resistance, higher glass transition temperature (Tg = 269.0 °C), breakdown strength (E_0 = 249.5 kV mm^{-1}), thermal stability ($T_{5\%}$ = 513.3 °C), dimensional resistance (CTE = 42.14 ppm $°C^{-1}$) and mechanical strength (98.81 MPa), which ensures the performance as the material for advanced ICs.

CRediT authorship contribution statement

Zhiyuan Peng: Conceptualization, Formal analysis, Investigation, Methodology, Software, Writing – original draft. **An Ye:** Conceptualization, Investigation, Software, Writing – original draft. **Ling Zhang:** Project administration, Supervision, Writing – review & editing. **Xiaolin Li:** Project administration. **Cheng Lian:** Supervision. **Chunzhong Li:** Funding acquisition, Project administration.

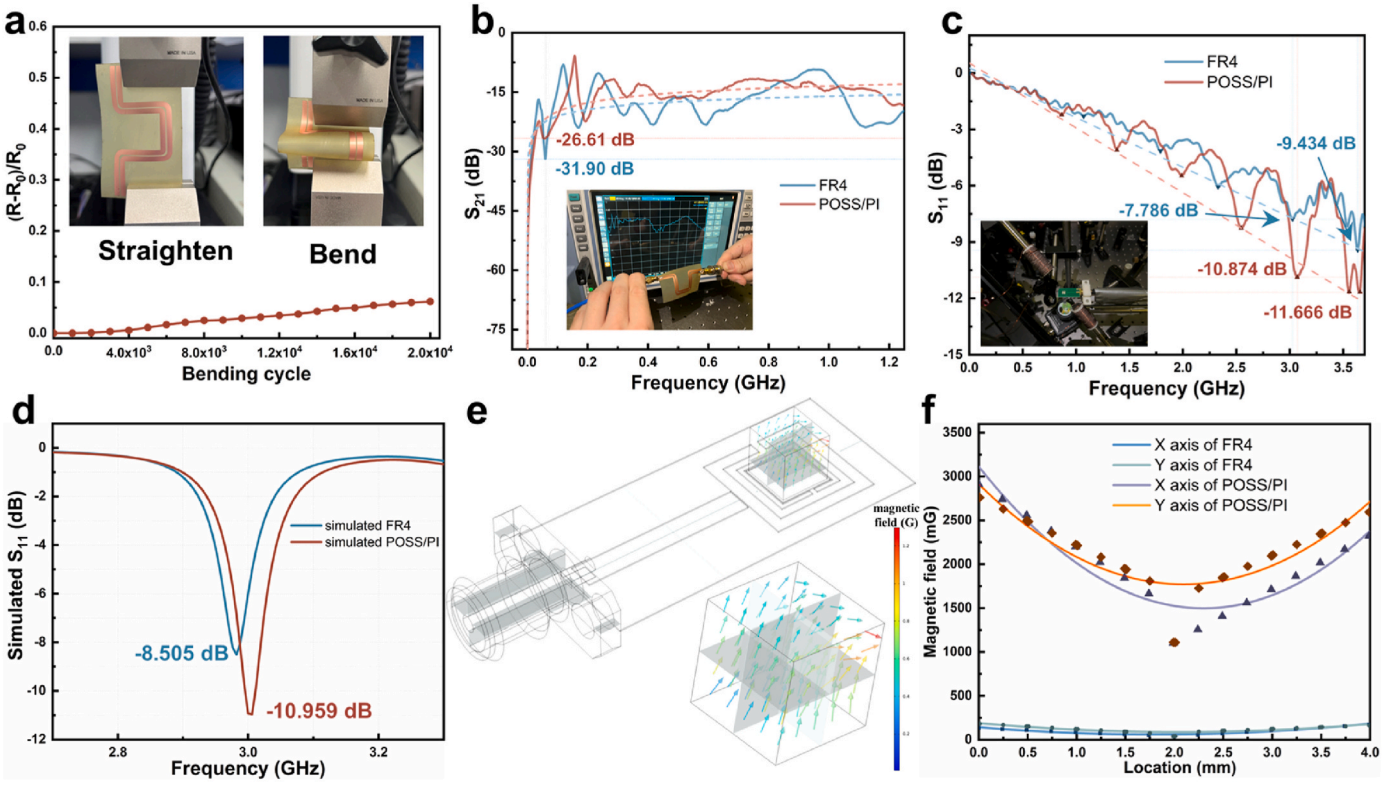

Fig. 4. a) Changes in resistance. b) S_{21} curves, c) S_{11} curves and d) simulated S_{11} with the substrate of FR4 and 3 wt% $8NH_2$-POSS/PI1. e) Images of simulated magnetic field in the 4 × 4 × 4 mm square region of 3 wt% $8NH_2$-POSS/PI1 substrate. The inset shows the region in detail. f) Simulated microwave magnetic field magnitude profile of the bottom xy plane.

Declaration of competing interest

The authors declare that they have no known competing financial interests or personal relationships that could have appeared to influence the work reported in this paper.

Data availability

Data will be made available on request.

Acknowledgments

This work was supported by the National Natural Science Foundation of China (22278140, U22B20143), the Science and Technology Commission of Shanghai Municipality (22DZ1205900), and the Fundamental Research Funds for the Central Universities.

Appendix A. Supplementary data

Supplementary data to this article can be found online at https://doi.org/10.1016/j.coco.2023.101804.

References

[1] D.-J. Liaw, K.-L. Wang, Y.-C. Huang, K.-R. Lee, J.-Y. Lai, C.-S. Ha, Advanced polyimide materials: syntheses, physical properties and applications, Prog. Polym. Sci. 37 (7) (2012) 907–974, https://doi.org/10.1016/j.progpolymsci.2012.02.005.
[2] L. Wang, C. Liu, S. Shen, M. Xu, X. Liu, Low dielectric constant polymers for high speed communication network, Advanced Industrial and Engineering Polymer Research 3 (4) (2020) 138–148, https://doi.org/10.1016/j.aiepr.2020.10.001.
[3] D. Ji, T. Li, W. Hu, H. Fuchs, Recent progress in aromatic polyimide dielectrics for organic electronic devices and circuits, Adv. Mater. 31 (15) (2019), https://doi.org/10.1002/adma.201806070.
[4] M. Kaltenbrunner, T. Sekitani, J. Reeder, T. Yokota, K. Kuribara, T. Tokuhara, M. Drack, R. Schwoediauer, I. Graz, S. Bauer-Gogonea, S. Bauer, T. Someya, An ultra-lightweight design for imperceptible plastic electronics, Nature 499 (7459) (2013) 458, https://doi.org/10.1038/nature12314.
[5] J.C. Sit, D.J. Broer, M.J. Brett, Liquid crystal alignment and switching in porous chiral thin films, Adv. Mater. 12 (5) (2000) 371, https://doi.org/10.1002/(sici)1521-4095(200003)12:5<371::Aid-adma371>3.0.Co;2-p. -+.
[6] Z.K. Zhu, J. Yin, F. Cao, X.Y. Shang, Q.H. Lu, Photosensitive polyimide/silica hybrids, Adv. Mater. 12 (14) (2000) 1055–1057, https://doi.org/10.1002/1521-4095(200007)12:14<1055::Aid-adma1055>3.0.Co;2-#.
[7] I. Gouzman, E. Grossman, R. Verker, N. Atar, A. Bolker, N. Eliaz, Advances in polyimide-based materials for space applications, Adv. Mater. 31 (18) (2019), https://doi.org/10.1002/adma.201807738.
[8] G. Maier, Low dielectric constant polymers for microelectronics, Prog. Polym. Sci. 26 (1) (2001) 3–65, https://doi.org/10.1016/s0079-6700(00)00043-5.
[9] C. Shi, S. Liu, Y. Li, Y. Yuan, J. Zhao, Y. Fu, Imparting low dielectric constant and high modulus to polyimides via synergy between coupled silsesquioxanes and crown ethers, Compos. Sci. Technol. 142 (2017) 117–123, https://doi.org/10.1016/j.compscitech.2017.02.002.
[10] W. Zhang, H. Jiang, Y. Nie, X. Fang, G. Chen, Composite films with low dielectric constant and dielectric loss factor at high frequency prepared from polyimide and polytetrafluoroethylene, Polym. Eng. Sci. 62 (12) (2022) 4226–4234, https://doi.org/10.1002/pen.26181.
[11] Y. Li, G. Sun, Y. Zhou, G. Liu, J. Wang, S. Han, Progress in low dielectric polyimide film - a review, Prog. Org. Coating 172 (2022), https://doi.org/10.1016/j.porgcoat.2022.107103.
[12] M.G. Dhara, S. Banerjee, Fluorinated high-performance polymers: poly(arylene ether)s and aromatic polyimides containing trifluoromethyl groups, Prog. Polym. Sci. 35 (8) (2010) 1022–1077, https://doi.org/10.1016/j.progpolymsci.2010.04.003.
[13] Z. Wu, J. He, H. Yang, S. Yang, Progress in aromatic polyimide films for electronic applications: preparation, structure and properties, Polymers 14 (6) (2022), https://doi.org/10.3390/polym14061269.
[14] S.D. Kim, S. Lee, J. Heo, S.Y. Kim, I.S. Chung, Soluble polyimides with trifluoromethyl pendent groups, Polymer 54 (21) (2013) 5648–5654, https://doi.org/10.1016/j.polymer.2013.08.057.
[15] J. Kim, S. Baek, J. Lee, S. Lee, C. Ahn, J. Kim, H. Han, Improvement of trade-off between mechanical properties and dielectric of polyimide with surface modified silica nanoparticle for wafer level packaging, J. Ind. Eng. Chem. 114 (2022) 438–445, https://doi.org/10.1016/j.jiec.2022.07.034.
[16] L. Zhai, S. Yang, L. Fan, Preparation and characterization of highly transparent and colorless semi-aromatic polyimide films derived from alicyclic dianhydride and aromatic diamines, Polymer 53 (16) (2012) 3529–3539, https://doi.org/10.1016/j.polymer.2012.05.047.
[17] L. Tao, H. Yang, J. Liu, L. Fan, S. Yang, Synthesis and characterization of highly optical transparent and low dielectric constant fluorinated polyimides, Polymer 50 (25) (2009) 6009–6018, https://doi.org/10.1016/j.polymer.2009.10.022.
[18] Z.-g. Fan, S.-w. Liu, Z.-g. Chi, Y. Zhang, J.-r. Xu, Construction and study of quantitative structure-property relationship model for intrinsic polyimide dielectric constant, Acta Polym. Sin. 52 (7) (2021) 750–761, https://doi.org/10.11777/j.issn1000-3304.2020.20278.
[19] X. He, S. Zhang, Y. Zhou, F. Zheng, Q. Lu, The "fluorine impact" on dielectric constant of polyimides: a molecular simulation study, Polymer 254 (2022), https://doi.org/10.1016/j.polymer.2022.125073.
[20] K. Zagorodniy, H. Hermann, M. Taut, Molecular design of ultralow-k insulator materials, Materials Science-Poland 25 (4) (2007) 1203–1211. <Go to ISI>://WOS:000253376600028.
[21] Z. Chen, Y. Zhou, Y. Wu, S. Liu, H. Huang, J. Zhao, Fluorinated polyimide with polyhedral oligomeric silsesquioxane aggregates: toward low dielectric constant and high toughness, Compos. Sci. Technol. 181 (2019), https://doi.org/10.1016/j.compscitech.2019.107700.
[22] B.B. Narzary, B.C. Baker, N. Yadav, V. D'Elia, C.F.J. Faul, Crosslinked porous polyimides: structure, properties and applications, Polym. Chem. 12 (45) (2021) 6494–6514, https://doi.org/10.1039/d1py00997d.
[23] D.-L. Zhou, J.-H. Li, Q.-Y. Guo, X. Lin, Q. Zhang, F. Chen, D. Han, Q. Fu, Polyhedral oligomeric silsesquioxanes based ultralow-k materials: the effect of cage size, Adv. Funct. Mater. 31 (31) (2021), https://doi.org/10.1002/adfm.202102074.
[24] J. Wang, J. Sun, J. Zhou, K. Jin, Q. Fang, Fluorinated and thermo-cross-linked polyhedral oligomeric silsesquioxanes: new organic-inorganic hybrid materials for high-performance dielectric application, ACS Appl. Mater. Interfaces 9 (14) (2017) 12782–12790, https://doi.org/10.1021/acsami.7b01415.
[25] K.N. Raftopoulos, K. Pielichowski, Segmental dynamics in hybrid polymer/POSS nanomaterials, Prog. Polym. Sci. 52 (2016) 136–187, https://doi.org/10.1016/j.progpolymsci.2015.01.003.
[26] S. Li, D. Xie, G. Qu, L. Yang, D. Min, Y. Cheng, Tailoring interfacial compatibility and electrical breakdown properties in polypropylene based composites by surface functionalized POSS, Appl. Surf. Sci. 478 (2019) 451–458, https://doi.org/10.1016/j.apsusc.2019.01.082.
[27] H. Zuo, Y. Chen, G. Qian, F. Yao, H. Li, J. Dong, X. Zhao, Q. Zhang, Effect of simultaneously introduced bulky pendent group and amide unit on optical transparency and dimensional stability of polyimide film, Eur. Polym. J. 173 (2022), https://doi.org/10.1016/j.eurpolymj.2022.111317.
[28] M. Çakir, E. Akin, Characterization of carbon fiber-reinforced thermoplastic and thermosetting polyimide matrix composites manufactured by using various synthesized PI precursor resins, Compos. B Eng. 231 (2022) 109559, https://doi.org/10.1016/j.compositesb.2021.109559.
[29] Y.-C. Chen, Y.-C. Lin, C.-C. Kuo, M. Ueda, W.-C. Chen, Investigation of the structure-dielectric relationship of polyimides with ultralow dielectric constant and dissipation factors using density functional theory, Polymer 256 (2022), https://doi.org/10.1016/j.polymer.2022.125184.
[30] J. Peng, Q. Wang, J. Wang, J. Yang, T. Jiang, G. Zeng, Structure and properties of low dielectric constant polyetherimide films containing-CF3 and cardo groups, Macromol. Res. 30 (11) (2022) 826–835, https://doi.org/10.1007/s13233-022-0089-6.
[31] H.-j. Ni, J.-g. Liu, Z.-h. Wang, S.-y. Yang, A review on colorless and optically transparent polyimide films: chemistry, process and engineering applications, J. Ind. Eng. Chem. 28 (2015) 16–27, https://doi.org/10.1016/j.jiec.2015.03.013.
[32] C. Ahn, T.Y. Kim, P.H. Hong, S. Choi, Y.-J. Lee, H. Kwon, H. Jeon, D.W. Ko, I. Park, H. Han, S.W. Hong, Highly transparent, colorless optical film with outstanding mechanical strength and folding reliability using mismatched charge-transfer complex intensification, Adv. Funct. Mater. 32 (20) (2022), https://doi.org/10.1002/adfm.202111040.
[33] S. Wang, Z. Luo, J. Liang, J. Hu, N. Jiang, J. He, Q. Li, Polymer nanocomposite dielectrics: understanding the matrix/particle interface, ACS Nano 16 (9) (2022) 13612–13656, https://doi.org/10.1021/acsnano.2c07404.
[34] Z. Hu, M. Liu, J. Che, Q. Kang, Z. Liu, Z. Qiang, X. Liu, Y. Xia, S. Huang, J. Zhang, Y. Chen, SLA printing of POSS-containing, bio-based composites with low dielectric constant and shape-memory function, Compos. Commun. 39 (2023) 101566, https://doi.org/10.1016/j.coco.2023.101566.
[35] Z.-H. Dai, T. Li, Y. Gao, J. Xu, Y. Weng, J. He, B.-H. Guo, Improved dielectric and energy storage properties of poly(vinyl alcohol) nanocomposites by strengthening interfacial hydrogen-bonding interaction, Colloids Surf., A 548 (2018) 179–190, https://doi.org/10.1016/j.colsurfa.2018.03.056.
[36] J. Chen, Y. Sun, W. Ge, Q. Shu, F. Min, Experimental investigation and DFT calculation of different amine/ammonium salts adsorption on oxidized coal, Chem. Phys. 561 (2022) 111598, https://doi.org/10.1016/j.chemphys.2022.111598.
[37] R. Borgani, L.K.H. Paon, M.S. Hedenqvist, U.W. Gedde, D.B. Haviland, Local charge injection and extraction on surface-modified Al2O3 nanoparticles in LDPE, Nano Lett. 16 (9) (2016) 5934–5937, https://doi.org/10.1021/acs.nanolett.6b02920.
[38] B. Du, J. Su, M. Tian, T. Han, J. Li, Understanding trap effects on electrical treeing phenomena in EPDM/POSS composites, Sci. Rep. 8 (2018), https://doi.org/10.1038/s41598-018-26773-y.
[39] M. Nagao, T. Hayashi, H. Imoto, K. Naka, Unsymmetric dumbbell-shaped polyhedral oligomeric silsesquioxane (POSS) compound as a single-component POSS hybrid, Langmuir 37 (50) (2021) 14777–14784, https://doi.org/10.1021/acs.langmuir.1c02906.
[40] B. Liu, B. Zhang, X. Wang, X. Chen, G. Gu, The preparation and properties of polyimide films modified by octa(aminopropylsilsesquioxane), J. Saudi Chem. Soc. 23 (7) (2019) 856–863, https://doi.org/10.1016/j.jscs.2019.02.002.

[41] I.E. Davidova, L.A. Gribov, I.V. Maslov, V. Dufaud, G.P. Niccolai, F. Bayard, J. M. Basset, Theoretical study of silsesquioxane organometallic complex structure and IR spectrum. II Interpretation of the IR spectrum, J Journal of Molecular Structure 443 (1) (1998).
[42] Z. Zhang, G. Liang, T. Lu, Synthesis and characterization of cage octa (aminopropylsilsesquioxane), J. Appl. Polym. Sci. 103 (4) (2007) 2608–2614, https://doi.org/10.1002/app.25304.
[43] X. Liu, J. Zhou, Y. Zhou, M. Wu, Y. Zhu, J. Zhao, S. Liu, H. Xiao, Chemically crosslinked polyimide-POSS hybrid: a dielectric material with improved dimensional stability and dielectric properties, Eur. Polym. J. 173 (2022), https://doi.org/10.1016/j.eurpolymj.2022.111315.
[44] W. Yan, X. Chen, J.S.K. Lim, H. Chen, V. Gill, A. Lambourne, X. Hu, Epoxy-assisted ball milling of boron nitride towards thermally conductive impregnable composites, Compos. Appl. Sci. Manuf. 156 (2022), https://doi.org/10.1016/j.compositesa.2022.106868.
[45] Y. Tang, P. Zhang, M. Zhu, J. Li, Y. Li, Z. Wang, L. Huang, Temperature effects on the dielectric properties and breakdown performance of h-BN/epoxy composites, Materials 12 (24) (2019), https://doi.org/10.3390/ma12244112.
[46] X.-J. Liu, M.-S. Zheng, G. Chen, Z.-M. Dang, J.-W. Zha, High-temperature polyimide dielectric materials for energy storage: theory, design, preparation and properties, Energy Environ. Sci. 15 (1) (2022) 56–81, https://doi.org/10.1039/d1ee03186d.
[47] J. Liu, L. Zhang, N. Wang, C. Li, Highly stretchable and transparent triboelectric nanogenerator based on multilayer structured stable electrode for self-powered wearable sensor, Nano Energy 78 (2020), https://doi.org/10.1016/j.nanoen.2020.105385.
[48] J. Liu, L. Zhang, C. Li, Highly stable, transparent, and conductive electrode of solution-processed silver nanowire-mxene for flexible alternating-current electroluminescent devices, Ind. Eng. Chem. Res. 58 (47) (2019) 21485–21492, https://doi.org/10.1021/acs.iecr.9b04329.
[49] P. Neumann, R. Kolesov, B. Naydenov, J. Beck, F. Rempp, M. Steiner, V. Jacques, G. Balasubramanian, M.L. Markham, D.J. Twitchen, S. Pezzagna, J. Meijer, J. Twamley, F. Jelezko, J. Wrachtrup, Quantum register based on coupled electron spins in a room-temperature solid, Nat. Phys. 6 (4) (2010) 249–253, https://doi.org/10.1038/nphys1536.
[50] G. Kucsko, P.C. Maurer, N.Y. Yao, M. Kubo, H.J. Noh, P.K. Lo, H. Park, M.D. Lukin, Nanometre-scale thermometry in a living cell, Nature 500 (7460) (2013) 54–U71, https://doi.org/10.1038/nature12373.
[51] F. Dolde, H. Fedder, M.W. Doherty, T. Noebauer, F. Rempp, G. Balasubramanian, T. Wolf, F. Reinhard, L.C.L. Hollenberg, F. Jelezko, J. Wrachtrup, Electric-field sensing using single diamond spins, Nat. Phys. 7 (6) (2011) 459–463, https://doi.org/10.1038/nphys1969.
[52] J.M. Taylor, P. Cappellaro, L. Childress, L. Jiang, D. Budker, P.R. Hemmer, A. Yacoby, R. Walsworth, M.D. Lukin, High-sensitivity diamond magnetometer with nanoscale resolution (vol 4, pg 810, Nat. Phys. 7 (3) (2008), https://doi.org/10.1038/nphys1937, 2011.
[53] M.W. Doherty, V.V. Struzhkin, D.A. Simpson, L.P. McGuinness, Y. Meng, A. Stacey, T.J. Karle, R.J. Hemley, N.B. Manson, L.C.L. Hollenberg, S. Prawer, Electronic properties and metrology applications of the diamond NV- center under pressure, Phys. Rev. Lett. 112 (4) (2014), https://doi.org/10.1103/PhysRevLett.112.047601.